JOURNAL OF CATALYSIS 34, 400–410 (1974)

A Model of Supported Metal Catalyst Sintering

II. Application of Model

PETER C. FLYNN* AND SIEGHARD E. WANKE†

Department of Chemical Engineering, The University of Alberta, Edmonton, Canada

Received February 6, 1974

An interparticle transport model for the sintering of supported metal catalysts is solved by finite difference methods and applied to several theoretical particle size distributions (PSD). The model predicts an increase in the rate of sintering as the width of the initial PSD increases. The rate of sintering also increases as the surface velocity and the metal loading increase. Sintering behavior is sensitive to the activation energy and temperature. Under certain conditions substantial redispersion is predicted.

The model can account for power-law orders from <2 to >13, as observed experimentally. Power-law order increases with PSD width and with increases in mean crystallite size.

NOMENCLATURE

a_0	Diameter of metal atom (0.277 nm for Pt)
D	Dispersion
F	Cumulative distribution function
$\bar{F}_s$	Average number of free surface atoms in time increment
K	Number of size increments used when generating initial PSD
l_i	Particle size, the length of the cube edge
l_{CRIT}	The particle size above which increase and below which decrease in size occurs (function of time)
l_{max}	The size of the largest particle in the initial PSD
l_{min}	The size of the smallest particle in the initial PSD
$N_{s,i}$	Number of surface metal atoms in crystallite i
P_k	Number particles assigned to size increments when generating initial PSD
q	The number of metal atom along cube edge minus one

Other nomenclature same as in Ref. (*1*).

* Present address: Syncrude Canada, Ltd., Edmonton, Alberta, Canada.

† To whom inquiries concerning this paper should be addressed.

INTRODUCTION

In a previous paper (*1*) we presented a model for the sintering of supported metal catalysts based on the dissociation of individual atoms from the metal crystallites, followed by migration of these atoms across the support surface and subsequent capture of these atoms by collision with metal crystallites. The equations that describe this process are [nomenclature same as in (*1*)]: the net rate of change of atoms per particle

$$\frac{dN_i}{dt} = \alpha v \frac{F_s}{N_t S_0} D_i - Ae^{-E_a/RT}, \qquad (1)$$

and the rate of change of the number of atoms migrating on the support surface

$$\frac{dF_s}{dt} = -\sum_{i=1}^{M} \frac{dN_i}{dt}. \qquad (2)$$

In the present paper solutions to Eq. (1) and (2) for various values of the param-

eters and different initial particle size distributions are presented. Comparisons of the predictions of the model with some experimental data are also made.

Method of Solution

Equations (1) and (2) were written in the following finite-difference form for solution

$$\Delta N_i = \left(\alpha v \frac{\bar{F}_s}{N_t S_0} D_i - A e^{-E_a/RT}\right) \Delta t, \quad (3)$$

$$\Delta F_s = -\sum_{i=1}^{M} \Delta N_i, \quad (4)$$

where

$$v = \left(\frac{\pi k_B T}{2m}\right)^{1/2} \quad (5)$$

$\bar{F}_s$ = arithmetic average of F_s during time increment Δt.

In the above formulation the constant α includes the reduction in the velocity of migrating atoms, v, due to an activation energy for surface diffusion. The support surface area per metal atom, S_0, is related to the metal loading of the catalyst. For example, $S_0 = 10$ nm^2/atom corresponds to a catalyst containing ~1 wt% Pt on a support having an area of 300 m^2/g.

Two methods of solution for Eqs. (3) and (4) were employed, depending on the value of α/S_0 [v being given by Eq. (5) and F_s/N_t, the fraction of atoms migrating on the support, being determined in part by the value of $\alpha v/S_0$].

1. $\alpha/S_0 > 10^{12}$ m^{-2}

For values of $\alpha/S_0 > 10^{12}$ m^{-2} it was found that F_s is always small, $F_s \simeq 0$, and the approximation $\Sigma_{i=1}^{M} \Delta N_i \simeq 0$, could be made. This condition corresponds to rapid rates of surface atom migration and capture compared to the rate at which atoms leave crystallites. For this situation, the rate at which a crystallite captures atoms, assuming all crystallites are equally accessible to migrating atoms, is proportional to diameter, D_i. Equations (3) and (4), for this case, reduce to

$$\Delta N_i = \left(\frac{MD_i}{\Sigma_{i=1}^{M} D_i} - 1\right) A e^{-E_a/RT} \Delta t. \quad (6)$$

The values of N_i, for all particles, as a function of time can readily be computed by a single-step method (Euler's formula) once a relationship between D_i and N_i is chosen. In this work we described the crystallites as fcc cubes and used the equations of Van Hardeveld and Hartog (*2*) to determine the total number of atoms, N_i, and the number of atoms, $N_{s,i}$, at the surface of each crystallite, i.e.,

$$N_i = 0.5 + 0.5[1 + 2q]^3 \quad (7)$$

and

$$N_{s,i} = 12q^2 + 2 \quad (8)$$

for $q \geq 1$
where

$$q = \frac{(l_i - a_0)}{2^{1/2} a_0}$$ (i.e., the number of atoms along the edge of cube minus one)

l_i = the length of the edge of cube
a_0 = atomic diameter (0.277 nm for Pt).

The effective diameter, D_i, of a crystallite for the capture of migrating atoms was taken as

$$D_i = 4(l_i + a_0). \quad (9)$$

By starting with a given particle size distribution, i.e., l_i for all particles at time = 0, Eq. (6) was used to obtain N_i's as a function of time. The corresponding dispersion, D, was calculated by

$$D = \frac{\Sigma_{i=1}^{M} N_{s,i}}{\Sigma_{i=1}^{M} N_i}. \quad (10)$$

Any crystallites for which N_i became <14 (i.e., $q < 1$) during a time interval were considered to have disappeared, and the remaining atoms in these crystallites were distributed among the remaining crystallites in the following time increment in proportion to their size.

2. $\alpha/S_0 < 10^{12}$ m^{-2}

For this range of α/S_0, F_s was substantial and the approximation $F_s \simeq 0$ was no

longer valid. Equations (3) and (4) were solved by the more tedious trial and error solution (which reduces to the Euler's solution described above for higher α/S_0 value). The number of atoms, F_s, was taken as zero at time equal to zero. In order to avoid oscillatory values of F_s in the initial time increments a heating period was incorporated in the calculations. The temperature was increased from 300°K to the desired final temperature over a period of 1 hr in 0.01 hr increments. The trial and error procedure used to calculate N_i and F_s at time $t' = t + \Delta t$ was as follows:

1. The value of F_s at t' was guessed (i.e., ΔF_s for Δt).
2. ΔN_i was computed for each particle using Eq. (3), where

$$\left(\bar{F}_s = F_s|_t + \frac{\Delta F_s}{2}\right).$$

3. ΔF_s was computed using Eq. (4).
4. If ΔF_s from step 1 differed from ΔF_s by step 3 by less than 0.1 atoms and if $F_s|_t + \Delta F_s$ was ≥ 0 calculation proceeded to the next time increment; if the difference was >0.1 steps 1 to 3 were repeated, with the new ΔF for step 1 being estimated using the magnitude of the difference as a guide.

If only a negative value of F_s (physically impossible) at t' could satisfy the above conditions, the size of Δt was decreased to one-tenth of its value and steps 1 to 4 were repeated. If any N_i became <14, these N_i were added to F_s in the next time increment.

The dispersion for this case was calculated in a manner analogous to Eq. (10), except that F_s was included in the number of metal surface atoms, i.e.,

$$D = \frac{F_s + \Sigma_{i=1}^{M} N_{s,i}}{\Sigma_{i=1}^{M} N_i}. \qquad (11)$$

A value of 0.1 hr for Δt was used for the reported results. In order to test the sensitivity of the results to the size of the time increment, calculations using a Δt of 0.017 hr were also carried out, yielding essentially the same results.

Description of Cases Investigated

1. Crystallite Size Distributions

The initial (zero-time) particle size distributions (PSD) were generated in the following manner:

1. The maximum and minimum size of particles in the distribution was chosen (l_{max} and l_{min}),
2. The size range was split into K equal size increments of size Δl,
3. The number of particles, P_k, was specified for each size increment,
4. The size of each particle was calculated by

$$l_i = l_{min} + (k-1)\Delta l + \left(\frac{j-1}{P_k}\right)\Delta l \qquad (12)$$

for $k = 1$ to $K + 1$ and $j = 1$ to P_k for each k. Where $i = j + \Sigma_{m=0}^{k-1} P_m$ with $(P_0 = 0)$, $P_{K+1} = 1$ was included to obtain a particle size of l_{max}. This procedure results in $\Sigma_{k=1}^{K+1} P_K$ particles all having a different size.

TABLE 1
Data for Generation of Particle Size Distributions

Distribution no.	l_{min} (nm)	l_{max} (nm)	Type	Dispersion
1	2.70	3.30	I	0.35
2	2.10	3.90	I	0.34
3	1.20	4.80	I	0.31
4	2.960	3.065	I	0.35
5	2.00	12.50	I	0.13
6	5.00	15.50	I	0.10
7	1.50	4.29	II	0.35
8[a]	1.50	4.29	II	0.28
9[a]	2.70	3.30	I	0.29

Type I

$$P_k = \begin{cases} k \text{ for } k = 1 \text{ to } 10 \\ 10 \text{ for } k = 11 \text{ and } 12 \\ 22 - k \text{ for } k = 13 \text{ to } 21 \\ 1 \text{ for } k = 22 \end{cases}$$

Type II

k	1	2	3	4	5	6	7	8	9	10
P_k	20	20	18	16	14	12	10	7	3	1

[a] One 10 nm particle was added to these distributions to simulate a bimodal distribution.

Two general types, I and II, of PSD were generated by this procedure. The Type I distribution is approximately Gaussian in nature, and Type II is skewed with a large fraction of small particles. The values of l_{min}, l_{max}, k and P_k used to generate the specific PSD are given in Table 1. (Only those PSD for which specific results will be presented are described in Table 1. Twenty other PSD with different l_{max} and l_{min} values were also examined.)

The PSD listed in Table 1 contain 121 particles, except 8 and 9 which contain 122. In these two distributions one large particle (10 nm) was added to PSD 1 and 7. To check the sensitivity of the calculations to the number of particles present, calculations were carried out with PSD for which the values of P_k for $k = 1$ to K were doubled (P_{K+1} was kept equal to one). These calculations showed that as long as the remaining number of particles was ≥ 7 the dispersion as a function of time remained unaltered.

2. Parameter values

The values of parameters used in solving Eqs. (3) and (4) [or Eq. (6)] for the specific cases reported in the next section are listed in Table 2. Although many other combinations of parameters were examined the cases listed illustrate the general behavior of the model. It should be mentioned that, although all the cases listed used a value of $A = 8 \times 10^{13}$ sec^{-1}, the results are readily extended to lower values of A (significantly higher values of A are physically unlikely). Thus, for a specific PSD and fixed values of T and α/S_0, the dispersion as a function of time is determined by the value of $A \exp(-E_a/RT)$, i.e., $A = 1.65 \times 10^7$ sec^{-1} and $E_a/RT = 15.0$ is equivalent to $A = 8 \times 10^{13}$ sec^{-1} and $E_a/RT = 35.0$ (Case 1).

TABLE 2
PARAMETER VALUES USED IN STUDY[a]

Case no.	E_a/RT	T (°K)	$\frac{\alpha}{S_0}$ (m^{-2})
1	35.0	1000	$>1 \times 10^{12}$
2	35.0	1000	2×10^7
3	33.3	900	$>1 \times 10^{12}$
4	33.0	900	2×10^7
5	31.6	950	$>1 \times 10^{12}$
6	31.6	950	2×10^9
7	31.6	950	2×10^7
8	31.6	950	4×10^6
9	31.6	950	2×10^6
10	30.0	1000	$>1 \times 10^{12}$
11	30.0	1000	2×10^7
12	27.5	1000	$>1 \times 10^{12}$

[a] $A = 8 \times 10^{13}$ sec^{-1} for all cases.

RESULTS AND DISCUSSION

1. Effect of Initial PSD on Rate of Sintering

From Eq. (1) it is evident that for a certain value of D_i, and the corresponding crystallite size, l_i, according to Eq. (9), the net rate of growth is equal to zero. Particles with sizes larger than this 'critical' size will grow while smaller particles will shrink. This critical size is given by

$$l_{CRIT} = \frac{AN_tS_0}{4\alpha v F_s} e^{-E_a/RT} - a_0 \qquad (13)$$

or according to Eq. (6)

$$l_{CRIT} = \frac{\Sigma_{i=1}^{M} D_i}{4M} - a_0 = \frac{\Sigma_{i=1}^{M} l_i}{M}. \qquad (14)$$

As sintering progresses the number of particles, M, decreases and the number of free surface atoms decreases as well. This results in an increase in l_{CRIT} as sintering progresses, and crystallites which initially grow in size will eventually decay.

Figure 1a and b shows the particle size history for individual particles of the same initial size for PSD 1 and 9, Case 3. PSD 1 and 9 are the same except one 10 nm particle has been added to PSD 1 to get PSD 9. The effect of the added 10 nm particle is evident when comparing Figure 1a and b. This large particle captures many of the migrating atoms, resulting in an increased rate of sintering.

The effect of large particles or broad initial PSD on the rate of sintering is further illustrated in Fig. 2 where the normalized dispersion D/D_0 is shown as a function of time for various initial PSD.

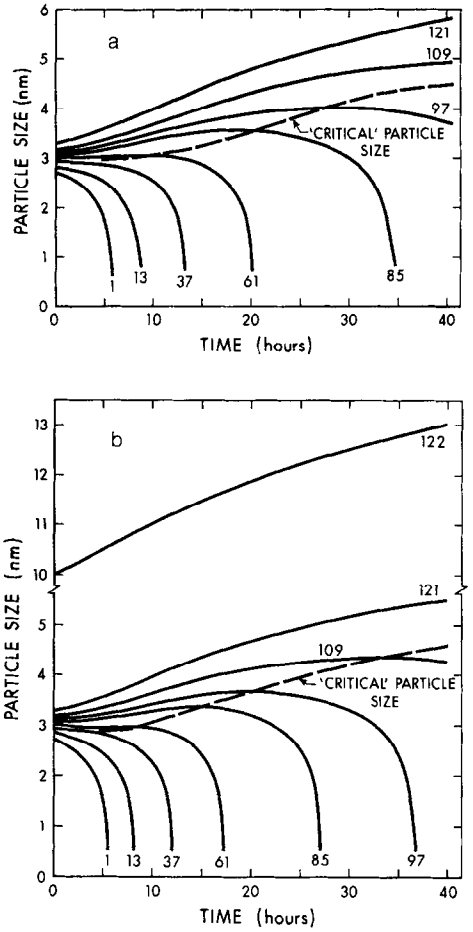

FIG. 1. Particle size history for selected individual particles (number is i, the particle number in the PSD): (a) PSD 1, Case 3; (b) PSD 9, Case 3.

The addition of one large particle (10 nm) to PSD 7 (i.e., to get PSD 8) significantly increases the rate of sintering. PSD 1 to 4 are all Type I distributions with a mean crystallite size of 3.0 nm, but the size range ($l_{max} - l_{min}$) varying from 0.105 nm (PSD 4) to 3.60 nm (PSD 3). The rate of sintering, as shown in Fig. 2, is larger for the broader distribution in an initial period of about 10 hr. The reduced rate of sintering for narrow distributions occurs because in the initial stages of sintering these distributions are becoming gradually broader without the disappearance of particles. The narrow size range does not generate a substantial driving force for transfer of metal from the smaller to the larger particles.

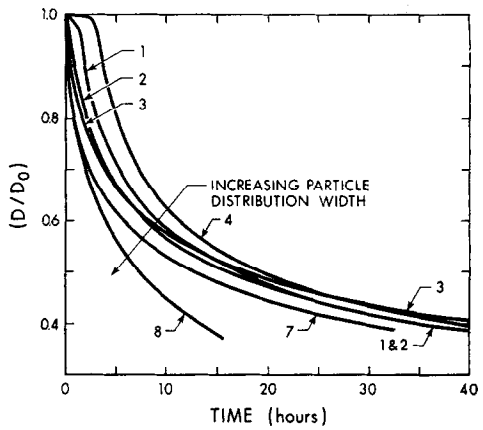

FIG. 2. Effect of initial particle size distribution on the rate of sintering (Case 5, the numbers identify the PSD).

Figure 3a and b shows the cumulative distribution function F as a function of time for Type I and II initial distributions. This illustrates the spreading of the distributions with time. In each case, as sintering progresses the model predicts the presences of particles smaller than the initial minimum size. During early stages of sintering the broadening, and specifically the decay of a substantial fraction of the particles to smaller sizes, is evident. This prediction of the presence of small particles at all stages of sintering is one significant difference between the proposed interparticle transport model and the crystallite diffusion model (*3*, *4*). The latter model does not allow for formation of particles smaller than the initial minimum size, nor does it predict the type of induction period for narrow PSD shown in Fig. 2.

2. The Effect of Surface Mobility and Metal Loading on Sintering Behavior

If no initial free surface atoms are postulated, then during the early stages of sintering the value of F_s grows as particles lose atoms to the surface and relatively few are captured by crystallites. The parameter α/S_0 determines the extent to which migrating surface atoms are captured, and hence the size of F_s. The initial increases in dispersion [as defined by Eq. (11)] shown in Fig. 4 are due to this increase in F_s.

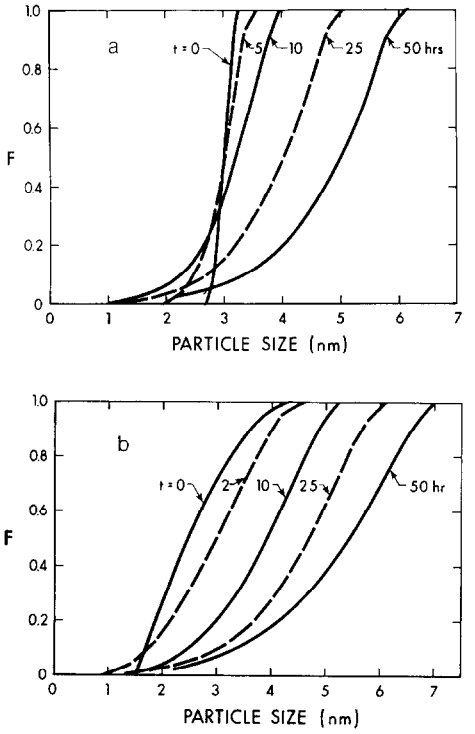

FIG. 3. Cumulative particle size distribution as a function of time, showing the broadening of the initial distribution: (a) PSD 1, Case 3; (b) PSD 2, Case 3.

For large values of α/S_0, corresponding to high metal loadings (i.e., small values of S_0) or high velocity of migration, the number of migrating surface species approaches zero and the rate of sintering is controlled by the loss from particles only. In these cases, the rise in dispersion due to the surface species is negligible, and this model does not predict any redispersion of metal.

Lower values of α/S_0, however, can account for significant redispersion. The lower parameter values could arise from lower metal loadings or a reduced velocity of migrating species (larger E_s). In such cases a significant amount of free surface atoms builds up, leading to substantially higher dispersions and reduced overall rates of sintering. Redispersion could occur through cooling of a sintering sample during this period of growth in number of free surface atoms. If the migrating atoms were frozen as single atoms or small particles during

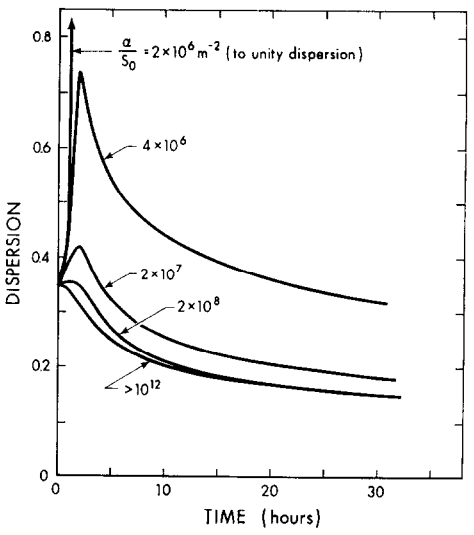

FIG. 4. Effect of surface mobility of metal atoms on support, and metal loading, on sintering behavior (PSD 1, Cases 5 to 9).

cooling, the increased dispersion would remain. Figure 4 shows that for α/S_0 values less than about $2 \times 10^6\ m^{-2}$ the capacity of the surface to accommodate free surface atoms exceeds the number of atoms present, and thus all the particles disappear.

The predictions of the model as α/S_0 becomes smaller may become unreliable because the assumption that the surface concentration of migrating atoms is position independent is no longer valid at low migration rates. The extent of the error introduced by this approximation has not been investigated.

3. *The Effect of E_a/RT on Sintering Behavior*

Figure 5a shows, for the case where α/S_0 is large and the free surface atoms are rapidly captured, the influence on sintering behavior of variations in E_a/RT. The plots correspond to either a change in temperature or in the activation energy. For instance, if E_a is taken as 60 kcal/g mole, the curves in Fig. 5a would represent temperatures ranging from about 850°K ($E_a/RT = 35$) to 1100°K ($E_a/RT = 27.5$). If the temperature is postulated as 1000°K, the curves represent activation energies from 55 to 70 kcal/g mole.

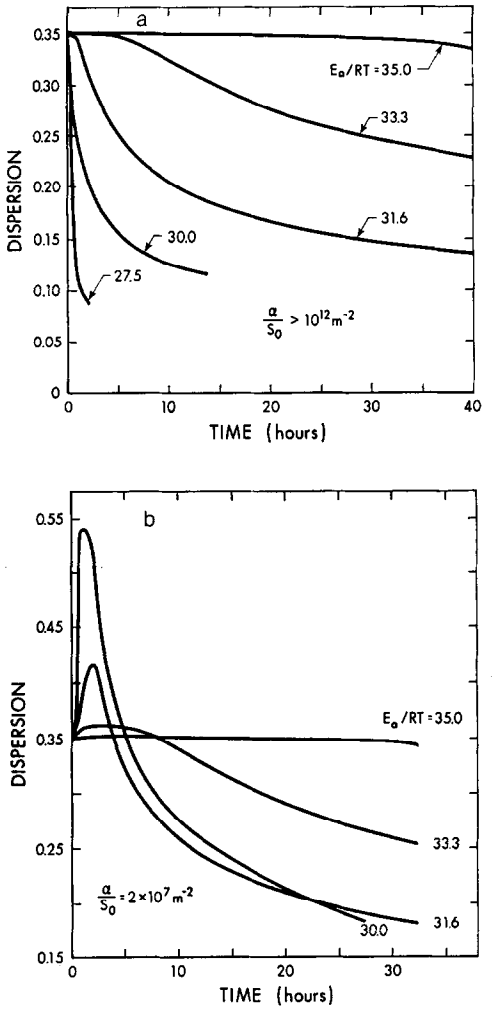

FIG. 5. Effect of E_a/RT on sintering behavior for PSD 1. (a) High value of α/S_0, Cases 1, 3, 5, 10 and 12; (b) low value of α/S_0, Cases 2, 4, 7 and 11.

As would be expected for such large activation energies, the sintering behavior is extremely sensitive to variations in temperature. Sintering is extremely slow for $E_a/RT = 35.0$, with less than 10% loss of dispersion in 40 hr, while for $E_a/RT = 27.5$, sintering is extremely rapid, resulting in the transfer of all the metal in the initial 121 particles to a single large particle within 5 hr.

Similar trends are evident, as shown in Fig. 5b, when values of α/S_0 are lower and a significant surface concentration of migrating atoms is present. In this case, however, a lower value of E_a/RT, corresponding to higher temperatures or a lower activation energy, affects not only the rate of sintering but also the extent of initial redispersion. While lower values of E_a/RT lead eventually to more rapid sintering, the initial rise means that for a period of time the dispersion is lower for higher E_a/RT values.

Changes in atmosphere would affect the activation energy for metal movement from the particle to the support surface. The actual species leaving would probably differ in oxidizing and reducing atmospheres. In the former case a metal oxide molecule would probably be the migrating species. Oxidizing atmospheres are found to enhance interactions between metal and support (*5*), and thus could lower the activation energy of escape. The pre-exponential factor, A, could also be affected. It is possible that in the case of oxidizing atmospheres the rate determining step in the sintering process is the formation of the surface oxide species since oxygen adsorption on metals such as Pt is an activated process. Different atmospheres could also affect the velocity of migration along the surface, i.e., changes in the activation energy for surface migration, a factor included in the parameter α discussed above.

4. The Order of Sintering

Several authors [e.g. (*6*, *7*)] have fit experimental data of sintering to a power-law model of the form

$$\frac{dD}{dt} = -KD^n, \qquad (15)$$

where D is the dispersion and K and n are constants. Values of n from 2 to 13 have been reported.

In this work we have fitted the rate of change of dispersion to Eq. (15) to determine the range of n values predicted by the proposed model. One immediate difficulty with the power-law model is its inability to account for an initial period of redispersion as the surface atom concentration builds up. Accordingly, we have fitted only those data for the regions where

the dispersion is decreasing. If Eq. (15) is valid, then a plot of $(D_0/D)^{n-1}$ versus time will result in a straight line with an intercept of unity ($n \neq 1$). Figure 6 shows these plots for PSD 5 and 6. These distributions are identical, except the mean size is displaced by 3.0 nm. The behavior for PSD 5 (mean size = 7.25 nm) is well fitted by an n value of 6, while PSD 6 (mean size = 10.25 nm) is well fitted by an n value of 3. This tendency of decreasing values of n with increasing mean particle sizes for symmetrical PSD was observed for several other PSD.

Figure 7 illustrates the effect of PSD width on the value of n for PSD with the same mean size (PSD 1 and 2). Neither case is well described by the power-law model, but the narrow PSD 1 shows very low values of n (<2) at times <15 hr. This is the result of the 'induction' period for the sintering behavior of narrow PSD that has been discussed previously. As PSD 1 broadens with time (see Fig. 3a) the value of n increases and at even larger values of time n decreases. A similar, but less marked, trend is observed with PSD 2. Not only does n vary with the extent of sintering, but the value of n also depends on the width of the initially symmetric PSD.

The inability of the power-law model to describe the progress of sintering over wide variations of D/D_0 is well recognized (*7*, *8*). It is evident that the sintering process should depend on the nature of the PSD and not only on the dispersion. The proposed model predicts the nature of the dependence of n on PSD, but experimental determinations of n as a function of PSD are not presently available.

5. Application of the Model to an Experimental Case

To test the ability of the proposed model to describe some experimental sintering

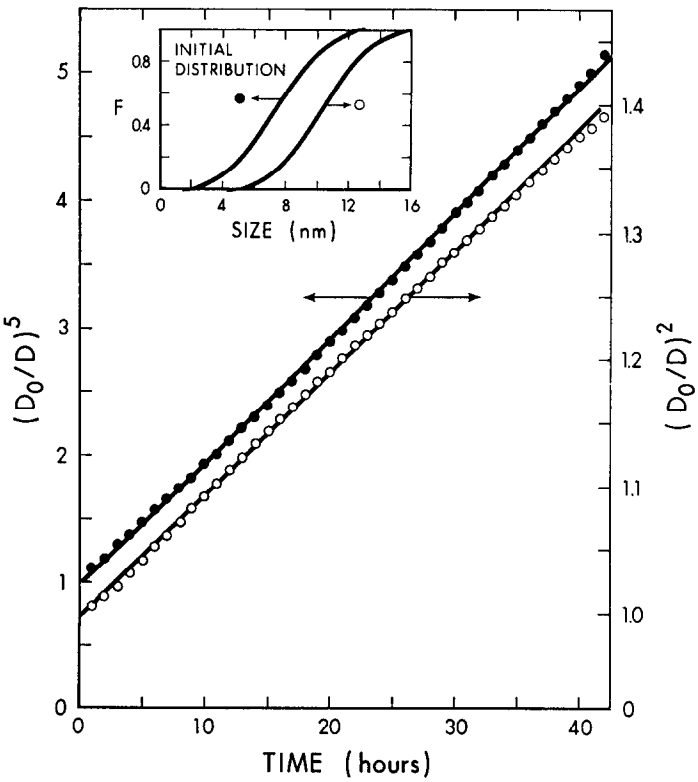

FIG. 6. Effect of mean crystallite size on power-law order (Case 5; (●) PSD 5, (○) PSD 6).

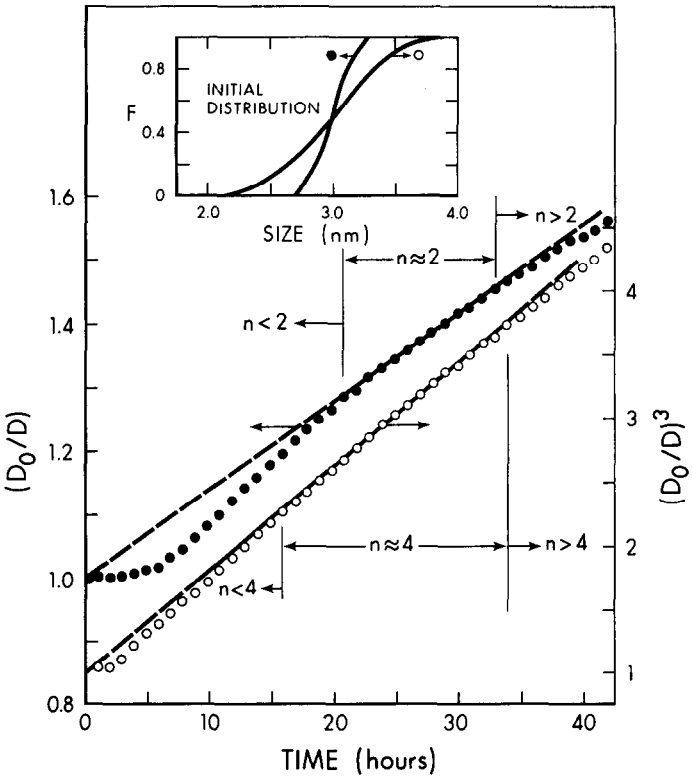

FIG. 7. Effect of particle size distribution width on power-law order (Case 3; (●) PSD 1, (○) PSD 2).

data we chose the data of Wynblatt and Gjostein (7). An approximate initial PSD was obtained by measuring the size of approximately 200 particles in Fig. 1a of Ref. (7). The distribution was adjusted to yield an average initial dispersion of 6.7% corresponding to the average particle radius of ~8.0 nm reported by Wynblatt and Gjostein. The resulting bimodal PSD is shown in Fig. 8 (line at $t = 0$).

Equation (7) (i.e., $\alpha/S_0 > 10^{12}$ m^{-2}) was used to predict the PSD as a function of time. The value of E_a/RT was adjusted until the predicted dispersion at 15 hr was equal to 5.4% (corresponding to the reported average radius of 10 nm after 15 hr). The value of E_a/RT that gave this desired result was 29.5, corresponding to an activation energy of 57 kcal/g mole at 973°K. The predicted PSD and dispersion as a function of time for this case are shown in Figs. 8 and 9, respectively. Fitting the dispersion versus time results by Eq. (15) resulted in values of $n = 13$ at $t < 17$ hr, to $n = 4$ for $t = 25$ to 50 hr. This is illustrated in Fig. 10.

This result agrees well with the experimentally observed n value of 13 (7). The initially broad and bimodal PSD is responsible for a high value of n at low time. As sintering progresses the bimodal nature

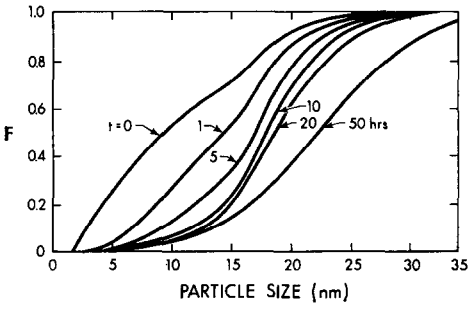

FIG. 8. Cumulative particle size distribution history predicted by model for the initial distribution (approximate) of Wynblatt and Gjostein [Ref. (7)].

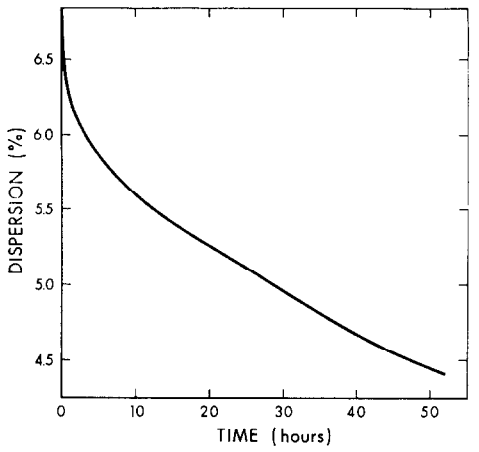

FIG. 9. Predicted dispersion as a function of time for the initial distribution of Wynblatt and Gjostein (7).

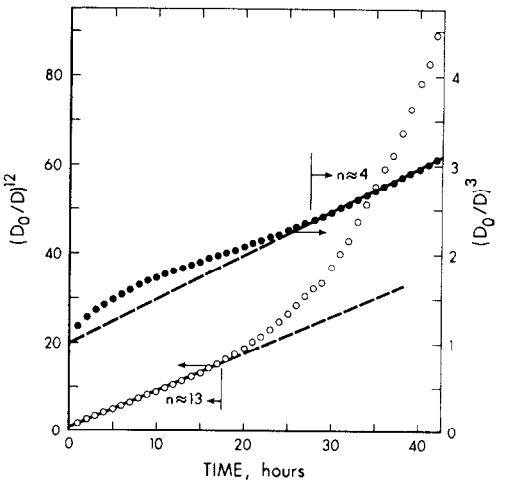

FIG. 10. A power-law order test of the calculated dispersion history for the initial distribution of Wynblatt and Gjostein (7), showing the fit to $n = 13$ for $t < 17$ hr and $n = 4$ for $t > 25$ hr.

of the distribution becomes less pronounced and at $t \simeq 20$ hr the PSD is approximately symmetric. As the PSD becomes more symmetric the value of n starts to decrease rapidly and changes from 13 to 4. To further test the validity of the model initial PSD and PSD as sintering progresses should be determined experimentally and compared to predictions.

CONCLUSIONS

An interparticle transport model of supported metal catalyst sintering has been developed and applied to a variety of simulated catalysts. The model can account for a wide variety of experimental observations of sintering. These include a strong influence of atmosphere, a high apparent activation energy, possible redispersion, and a variation in order from <2 to ≥ 13 when sintering behavior is fitted to a simple power-law equation.

The model predicts that the rate of sintering increases with increasing width of the initial PSD. Metal is transported from small to large particles, and transport is more rapid as the difference in size of particles is increased. This model predicts the presence of particles smaller than the initial minimum particle size as sintering progresses.

During the early stages of sintering the model predicts a buildup of a concentration of migrating metal atoms or molecules. If this buildup is substantial then redispersion of the catalyst will be significant. Factors affecting the extent of surface species buildup are migration velocity, collision accommodation, activation energy for escape from the particle to the support surface, temperature and metal loading. The first three factors would be influenced by the atmosphere in which sintering occurs.

This model predicts a considerable variation in order of fit to a power-law equation of sintering. Variation of the order is predicted within a given sintering experiment. Distribution width and initial particle size are especially critical parameters with respect to the power-law order.

A variety of improvements to the presented model can be made, such as: (a) using the Kelvin equation to calculate the rate of loss of atoms from larger crystallites rather than approximating this by a constant rate of loss per crystallite, (b) including variations in the concentration of migrating atoms with position, and (c) modeling the support surface as inhomogeneous. It is felt that at the present time improvements in the model along the above lines are unwarranted because insufficient

information is available to *a priori* estimate the extra parameters in these extended models. These new parameters, such as interfacial tensions, energy distribution of inhomogeneous support surface, etc., in the refined models would be determined by fitting them to experimental data and any improvement in the fit over the simple model would be due to an increase in the number of adjustable parameters. One of the strengths of the presented model is that it contains only three parameters, i.e., α, A, and E_a (in the case of Eq. (6) A and E_a are the only adjustable parameters), and it is easier to assign physical significance to these parameters and hence use their magnitude in designing catalysts with greater stability.

Acknowledgments

One of us (P. C. F.) gratefully acknowledges the support of an International Nickel Co. Graduate Fellowship. We also appreciate the support of this research by the National Research Council of Canada.

References

1. Flynn, P. C., and Wanke, S. E., *J. Catal.* **34**, 390 (1974).
2. Van Hardeveld, R., and Hartog, F., *Surface Sci.* **15**, 189 (1969).
3. Ruckenstein, E., and Pulvermacher, B., *AIChE J.* **19**, 356 (1973).
4. Ruckenstein, E., and Pulvermacher, B., *J. Catal.* **29**, 224 (1973).
5. Geus, J. W., *in* "Chemisorption and Reactions on Metallic Films" (J. R. Anderson, Ed.), Chap. 3. Academic Press, London, 1971.
6. Herrmann, R. A., Adler, S. F., Goldstein, M. S., and De Baun, R. M., *J. Phys. Chem.* **65**, 2184 (1961).
7. Wynblatt, P., and Gjostein, N. A., *Scr. Met.* **7**, 969 (1973).
8. Somorjai, G. A., *in* "X-Ray and Electron Methods of Analysis" (H. van Olphen and W. Parrish, Eds.), Chap. 6. Plenum, New York, 1968.